Distributed Control of Islanded Series PV-Battery-Hybrid Systems with Low Communication Burden

Pan, Yiwei; Yang, Yongheng; Blaabjerg, Frede

Published in:
2020 IEEE 11th International Symposium on Power Electronics for Distributed Generation Systems, PEDG 2020

DOI (link to publication from Publisher):
10.1109/PEDG48541.2020.9244482

Publication date:
2020

Document Version
Accepted author manuscript, peer reviewed version

A Decentralized Control for Islanded Series PV-battery Hybrid Systems with Low Communication Burden

Yiwei Pan, Yongheng Yang, and Frede Blaabjerg
Department of Energy Technology
Aalborg University
Aalborg, Denmark
{ypa, yoy, fbl}@et.aau.dk

***Abstract*—To better integrate distributed energy sources, the series photovoltaic-battery-hybrid (PVBH) system has been proposed. However, the state-of-the-art control highly relies on the communication, by which real-time control variables should be transmitted among all converters. To overcome this, a novel decentralized control method is proposed in this paper. Firstly, a PQ decoupling control is introduced, which enables the control of individual converters with only local measurements. Then, a reactive power distribution method is developed to achieve approximately equal power sharing among the hybrid converters. Additionally, two anti-over-modulation (AOM) loops are developed to address the over-modulation issue. With the proposed method, only the total power of the series system should be transmitted, and the communication burden can be significantly reduced. Simulation results have validated the effectiveness of the proposed method.**

***Keywords*—Decentralized control, power control, series-connected converters, PV-battery systems.**

I. INTRODUCTION

In recent years, the series structure has received growing interest in integrating distributed energy sources [1]-[4]. With this, the distributed low-voltage (LV) resources can be directly interfaced to separate DC rails of the series converter without an additional boost stage [1]. This will bring about several benefits such as reduced cost, improved efficiency, and modular design of the distributed energy systems. However, in most applications, the series system was centralized controlled with the adoption of high-bandwidth communications [2]-[4], which greatly increases the cost and reduces the reliability of the distributed system. Therefore, efforts have been made towards the decentralized control of the series system [1], [5]-[12].

In [1], a hierarchical control scheme was developed to achieve schedulable power for the series system, where a central controller was responsible for the voltage control of the point of common coupling (PCC), and local controllers were in charge of the power regulation of individual converters. However, this control is highly dependent on the low-bandwidth communication (LBC) system, by which many control variables should be real-time transmitted between the central and local controllers, leading to poor fault tolerance and reliability. To reduce the communication burden, an inverse power factor (PF) droop control and *f-P/Q* droop control were proposed in [5] and [6], respectively. Nevertheless, the unequal power sharing cases have not been addressed in these two methods. More importantly, in these methods, only ideal or same kind of DC sources were plugged into each DC rail of the series system. When different kinds of LV sources are interfaced to each DC rail, these methods cannot be directly implemented. Another control scheme with less LBC dependency is the current-/voltage-mode (CVM) control scheme [7], [8], where one or several converters are centralized controlled as a current source to regulate the line current of the series system, and others are controlled in a distributed way as voltage sources. With this method, the communication burden can be reduced to some extent [8]. However, only the grid-connected operation of the system with unity power factor (PF) was addressed in this method, while the islanded operation has not been discussed. In addition, due to the unequal power sharing, over-modulation may appear for all converter cells, possibly leading to instability.

On the other hand, since energy storage elements such as batteries can be equipped with PV systems to compensate for the fluctuation of solar energy, the series PV-battery-hybrid (PVBH) systems have been discussed in the recent literature [3], [9]-[12]. In [9] and [10], power control and balancing methods were developed to achieve schedulable power for the series PVBH systems based on the hierarchical control structure in [1]. The grid-connected operation of the PVBH system has also been discussed in [11] and [12] using the CVM control, where a ramp-rate and a virtual inertia control has been proposed for the battery cell to mitigate PV power variations, respectively. However, since these methods were similar with [7] and [8], similar issues also exist for these control methods, as discussed above.

To overcome the above limitations, a novel decentralized control is proposed in this paper for the islanded operation of series PVBH systems. By the proposed control, the PV panels can contribute as much power as possible, while the battery automatically regulates the voltage and frequency of the islanding grid according to the load demand. Reactive power can be shared in a way to balance the loading of all converters. To guarantee the stable operation of the system, two anti-over-modulation (AOM) loops are developed. With the proposed control, only a few variables with low dynamics should be transmitted to each controller through the LBC system, significantly reducing the communication burden.

The paper is organized as follows. In Section II, a PQ decoupling control is proposed, which enables the individual active and reactive power control with only local measurements. In Section III, a reactive power distribution method is

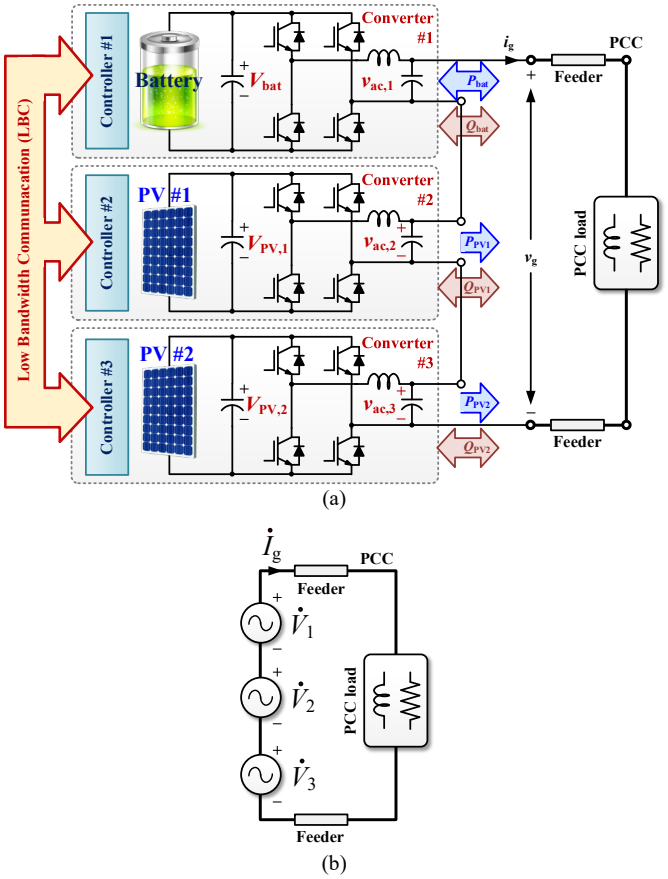

Fig. 1. (a) Topology and (b) equivalent circuit of a 3-cell series PVBH system, where $V_{ac,k}$ and $V_{ac,bat}$ are the AC voltages of the k^{th} converter cell and the battery cell, respectively. $V_{PV,m}$ and V_{bat} are the DC voltages of PV #m and the battery, respectively. v_g is the grid voltage.

introduced to realize approximately equal power sharing among all converters. In Section IV, the over-modulation issues of the series PVBH system is analyzed, and two anti-over-modulation (AOM) loops are developed to ensure the stable operation of the system. The effectiveness of the proposed decentralized control is then validated by simulations and experiments in Section V. Finally, concluding remarks are made in Section VI.

II. Proposed Decentralized Control

A. PQ decoupling control for PV converters

To illustrate the proposed control, an islanded 3-cell series PVBH system is exemplified in Fig. 1(a), where two PV converters and one battery converter are connected in series for the islanded grid. In the analysis below, assuming only one battery converter is equipped for the PVBH system. Since the output voltage of each cell can be individually controlled, the equivalent circuit of the 3-cell series PVBH system can be obtained as Fig. 1(b). It can be clearly observed that the same line current i_g flows through all cells, while the output voltage of each cell can be different from each other both in amplitude and phase angle. The phasor diagram of Fig. 1(b) is shown in Fig. 2, where the grid voltage vector $\dot{V}_g$ is synthesized by voltage vectors $\dot{V}_1$, $\dot{V}_2$ and $\dot{V}_3$. As shown in Fig. 2, the increment of $|\dot{V}_1|$ (the amplitude of $\dot{V}_1$) will lead to the increase of

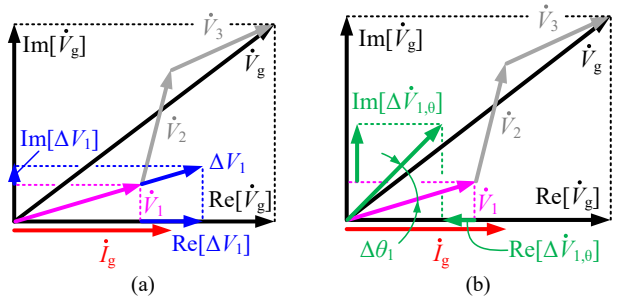

Fig. 2. Phasor diagram of a 3-cell series system when (a) the output voltage amplitude of converter #1 varies, and (b) the phase angle of converter #1 varies.

both active and reactive power of cell #1, while the increase of the PF angle θ_1 will results in the decrease of the active power and increase of the reactive power. According to Fig. 2, approximating $\sin\Delta\theta_k \approx \Delta\theta_k$ and $\cos\Delta\theta_k \approx 1$ ($\Delta\theta_k$ denotes the PF increment of the k^{th} converter), the relationship between the power and voltage phasor of the k^{th} converter can be described as

$$\begin{bmatrix}\Delta P_k \\ \Delta Q_k\end{bmatrix} = I_g \begin{bmatrix}\cos\theta_k & -V_k\sin\theta_k \\ \sin\theta_k & V_k\cos\theta_k\end{bmatrix}\begin{bmatrix}\Delta V_k \\ \Delta\theta_k\end{bmatrix} = I_g A \begin{bmatrix}\Delta V_k \\ \Delta\theta_k\end{bmatrix} \quad (1)$$

where ΔP_k, ΔQ_k, and ΔV_k are the increment of the active power, reactive power and voltage phasor amplitude of the k^{th} converter, respectively. A is the coupling matrix. From (1), it can be clearly observed that the variation of ΔV_k and $\Delta\theta_k$ will affect both the active and reactive power of the k^{th} cell, and this coupling relationship is dependent on the power factor of the k^{th} cell. Therefore, different from parallel distributed power converters, the conventional P/f and Q/V droop control cannot be directly implemented in the series system to realize the individual power control of each converter. It thus calls for a new decentralized control method.

To regulate the individual active/reactive power of each cell, by solving the inverse matrix of A, (1) can be rewritten as

$$\begin{bmatrix}\Delta V_k \\ \Delta\theta_k\end{bmatrix} = \frac{A^{-1}}{I_g}\begin{bmatrix}\Delta P_k \\ \Delta Q_k\end{bmatrix} = \frac{1}{I_g}\begin{bmatrix}\cos\theta_k & \sin\theta_k \\ -\dfrac{\sin\theta_k}{V_k} & \dfrac{\cos\theta_k}{V_k}\end{bmatrix}\begin{bmatrix}\Delta P_k \\ \Delta Q_k\end{bmatrix} \quad (2)$$

According to (2), a PQ decoupling control can be obtained, as shown in Fig. 3(a), being the overall control diagram of the PV converter cell. As shown in Fig. 3(a), the active power of the PV converter cell is regulated by controlling the PV voltage V_{PV}, with its reference decided by the MPPT controller. Both the DC voltage and reactive power are regulated by proportional-integral (PI) controllers, and through the decoupling matrix, the increment on the amplitude and frequency of the output voltage can be calculated. The reference of the output voltage of the kth converter $V_{ac,k}$ is calculated by

$$v_{ac,k}^* = V_k^* \sin\left(\int \omega_k^* dt\right) = \left(\frac{V_{g,nom}}{n} + \Delta V_k\right)\sin\left(\int(\omega_{nom} + \Delta\omega_k)\,dt\right) \quad (3)$$

where $V_{g,nom}$ and ω_{nom} are the nominal amplitude and frequency of the grid voltage, respectively. n is the cascaded cell number.

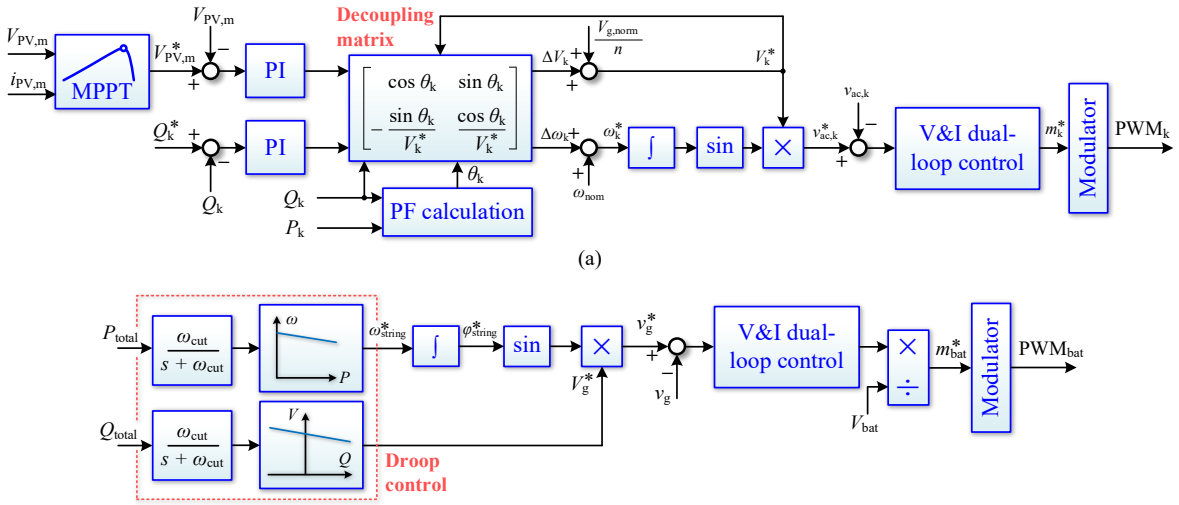

Fig. 3. Control diagrams of (a) the PV converter and (b) the battery converter. Here, the subscript "PV,m" denotes the PV#*m*, φ_{string} is the integration of ω_{string}.

$\Delta\omega_{\text{k}}$ is the increment on the frequency of the output voltage. Then, through the conventional voltage/current dual-loop control, both MPPT and reactive power control can be realized with only local measurements for the PV converter.

B. Droop control for the battery converter

As the system should participate in regulating the voltage/frequency of the islanding grid while compensating the PV power variations, the control diagram of the battery cell can thus be designed, as shown in Fig. 3(b), where the battery converter maintains the output voltage of the entire system following the droop curves. The amplitude and frequency references of the entire system, denoted as ω^*_{string} and V^*_{g}, respectively, are obtained as

$$\begin{cases} \omega^*_{\text{string}} = \omega_0 - k_{\text{d,p}} P_{\text{total}} \left(\dfrac{\omega_{\text{cut}}}{s+\omega_{\text{cut}}} \right) \\ V^*_{\text{g}} = V_{\text{g,0}} - k_{\text{d,q}} Q_{\text{total}} \left(\dfrac{\omega_{\text{cut}}}{s+\omega_{\text{cut}}} \right) \end{cases} \tag{4}$$

The voltage reference for the entire system is calculated by

$$v^*_{\text{g}} = V^*_{\text{g}} \sin\left(\int \omega^*_{\text{string}} \text{d}t \right) \tag{5}$$

where ω_0 and $V_{\text{g,0}}$ are the output voltage angular frequency and amplitude at no load, and $k_{\text{d,p}}$ and $k_{\text{d,q}}$ are the droop coefficients for the frequency and amplitude, respectively. ω_{cut} is the cut-off frequency of the low-pass filters (LPFs), which are employed in P/Q measurements. Then, through the voltage/current dual-loop control, the output voltage of the series system can be maintained by the battery converter. In this way, the external characteristics of the series system will behave like a droop-controlled power source, while the battery operates as a buffer to compensate the differential power between the load and the PV power generation.

C. Reactive power distribution

The reactive power of the entire system is distributed in a way to keep the apparent power of all converters approximately equal. To reduce the communication burden as much as possible, only the total active and reactive power are transmitted by the LBC. Thus, each converter only knows its own active power and the total power. In this case, the reactive power reference of each converter can be decided by assuming: 1) the apparent power for all converter cells is identical, and 2) the voltage phasors of other converter cells synthesize the total voltage phasor $P_{\text{total}} + \text{j}Q_{\text{total}}$ with the minimum amplitudes. With the above assumption, the relationship between the power of the PV converter and the total power can be described as

$$\frac{\left| P_{\text{PV,m}} + \text{j}Q_{\text{PV,m}} \right|}{\left| \left(P_{\text{total}} - P_{\text{PV,m}} \right) + \text{j}\left(Q_{\text{total}} - Q_{\text{PV,m}} \right) \right|} = \frac{1}{(h-1)} \tag{6}$$

Here, h equals to n (the cascaded number of the series system). This relationship is also illustrated in Fig. 4. Subsequently, the reactive power reference can be derived as

$$Q^*_{\text{k}} = \begin{cases} 0, & \sigma \le 0 \\ \dfrac{\sqrt{\sigma} - Q_{\text{total}}}{h^2 - 2h}, & \sigma > 0 \text{ and } \left| \sqrt{\sigma} - Q_{\text{total}} \right| < \left| -\sqrt{\sigma} - Q_{\text{total}} \right| \\ \dfrac{-\sqrt{\sigma} - Q_{\text{total}}}{h^2 - 2h}, & \sigma > 0 \text{ and } \left| \sqrt{\sigma} - Q_{\text{total}} \right| > \left| -\sqrt{\sigma} - Q_{\text{total}} \right| \end{cases}, \tag{7}$$

where

$$\sigma = Q^2_{\text{total}} - \left(h^2 - 2h \right) \left[(h-1)^2 P^2_{\text{k}} - \left(P_{\text{total}} - P_{\text{k}} \right)^2 - Q^2_{\text{k}} \right] \tag{8}$$

Moreover, the reactive power reference should be limited in a certain range as

$$Q^*_{\text{k}} = \begin{cases} Q_{\text{total}}, & \text{if abs}\left(Q_{\text{total}} \right) < \text{abs}\left(Q^*_{\text{k}} \right) \\ 0, & \text{if sgn}\left(Q_{\text{total}} \right) \ne \text{sgn}\left(Q^*_{\text{k}} \right) \end{cases} \tag{9}$$

to avoid excessive and reversed reactive power contribution.

Nevertheless, in general, the voltage phasors of other converters cannot exactly be the phasors with minimum

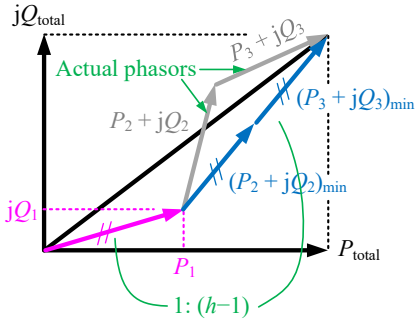

Fig. 4. Illustration of the reactive power distribution. where $P_{PV,m}$, and $Q_{PV,m}$ are the active and reactive power for the converter with PV#*m*, and P_{bat} and Q_{bat} denote the active and reactive power for the battery converter.

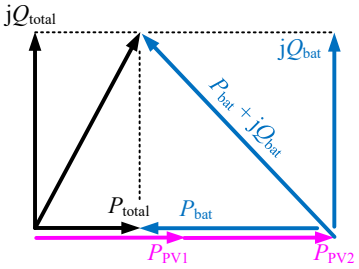

Fig. 5. Phasor diagram of the over-modulation caused by low PF.

amplitude, as illustrated in Fig. 4. Consequently, the power loading of the battery cell may be higher than PV converters. To address this, h can be set as a non-integer smaller than N, e.g., $h = 2.8$ for a 3-cell system. In this way, the PV converters can contribute more reactive power, and the power loading for the battery cell can be reduced.

With the decentralized control discussed above, individual active/reactive power control can be achieved for each converter in the series PVBH system. Only the total active and reactive power should be transmitted by the LBC for the reactive power distribution control. Compared with the conventional methods in [1], [9], [10], the communication burden is significantly reduced.

III. Over Modulation Issues

For the series system, there are three potential reasons that may lead to over-modulation of some converter cells, which are explained as follows:

1) Line current reduction: The over-modulation induced by the line current reduction has been discussed in [13]. Due to the MPPT control, when the line current reduces, the output voltage of the PV converter will have a higher magnitude to keep operating at MPP. This may lead to over-modulation of the PV converters.

2) Lower PF: As shown Fig. 5, if the reactive power of the series system is large while the active power is small, since the PV cells are operating in the maximum power tracking (MPPT) mode, hardly any reactive power will be contributed by the PV converters according to (7). In this case, the battery cell should not only absorb the surplus active power from PVs, but also independently provide all the reactive power. Therefore, the battery converter will be risky of over-modulation.

To address these two over-modulation issues, two AOM

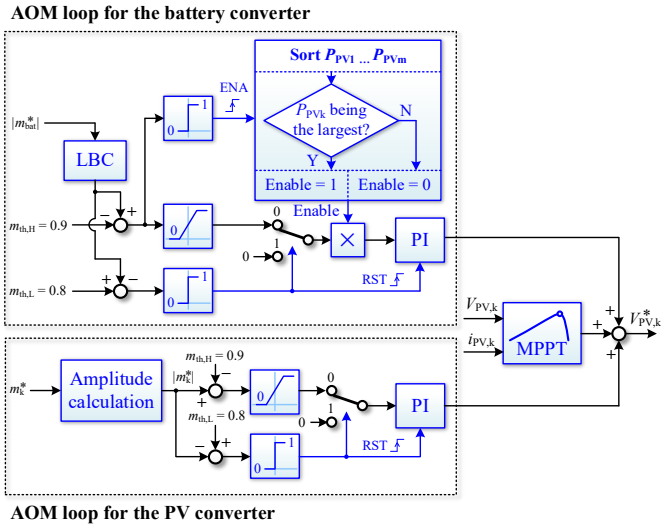

Fig. 6. Two anti-over-modulation loops.

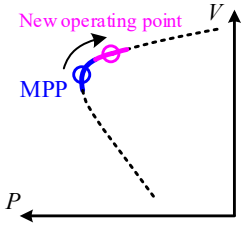

Fig. 7. Basic principle of the AOM control (MPP – maximum power point).

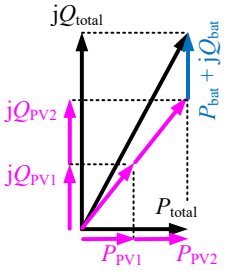

Fig. 8. Phasor diagram of the over-modulation caused by low PF with AOM control.

loops are developed, as shown in Fig. 6. The basic idea of the AOM loops is to discard part of the PV power by migrating the operating points of PVs from their MPPs to higher voltage region, as shown in Fig. 7. This effort has three benefits:

1) The magnitudes of the modulation indices for PV converters will be reduced due to the reduction of PV power.

2) The available DC voltages will become higher for PV converters, making the series system able to generate a higher AC voltage [10].

3) The reduction of PV power will reduce the charging power of the battery converter, if it is in the charging mode. As shown in Fig. 8, as the reduction of the PV power, PV converters will contribute more reactive power, compared to Fig. 5. As a result, the voltage phasor amplitude of the battery converter can be reduced.

The first AOM loop is designed to address the over-modulation issues of the PV converters. As shown in Fig. 6, if

TABLE I
PARAMETERS OF THE SERIES PVBH SYSTEM.

PV rated power	640 W
DC link capacitor	680 μF
Output LC filter	1.8 mH / 30 μF
Switching frequency of one cell	5 kHz
Controller sampling frequency	10 kHz
Nominal grid voltage (RMS) $V_{g,nom}$	220 V
Nominal grid frequency ω_{nom}	2π·50 rad/s
MPPT sampling rate	10 Hz
MPPT step-size	3 V
Nominal battery voltage	192 V
Total feeder impedance	0.04 Ω / 100 μH
P/f Droop coefficient $k_{d,p}$	0.0001 rad/W
Q/V Droop coefficient $k_{d,q}$	0.005 V/var
LPF cut-off frequency ω_{cut}	5 rad/s
Reactive power distribution coefficient h	2.8

$|m_k^*|$ (the amplitude of the modulation index for PV converter #k) is higher than a threshold $m_{th,H}$, which means that the PV converter is under the risk of over-modulation, a voltage increment will be added on the PV voltage reference, which is calculated by a PI controller. When $|m_k^*|$ reduces, e.g., lower than a threshold $\underline{m}_{th,L}$, which is lower than $m_{th,H}$, it means that the PV converter is free from the over-modulation risk. Subsequently, the PI regulator will be reset, and the PV converter starts to operate in the MPPT mode.

The AOM loop for the battery converter is similar. As shown in Fig. 6, if $|m_{bat}^*|$ (the amplitude of the modulation index for the battery converter) is higher than $m_{th,H}$, while the power of PV #k is the highest among all PV converters, then an increment from a PI regulator is added on the voltage reference of PV #k. In the proposed AOM loop, only the PV with the highest power will be selected to discard part of power. On the other hand, if $|m_{bat}^*|$ is lower than $\underline{m}_{th,L}$, the PI regulator will be reset, which indicates that the battery converter is free from the over-modulation risk.

Due to the introduction of these two AOM loops, more variables should be transmitted by the LBC, which are $|m_{bat}^*|$ and the PV power information, as shown in Fig. 6. Nevertheless, as the AOM loops and the transmitted variables have slow dynamics, and the LBC system will still be sufficient. Therefore, the AOM loops has minor impact on the communication burden of the series system.

IV. VALIDATION RESULTS

A. Simulation Results

To validate the effectiveness of the proposed method, simulations on a 3-cell PVBH system shown in Fig. 1 are performed in the MATLAB/Simulink. The parameters of the simulation are shown in Table I. Three cases have been considered to demonstrate the performance of the proposed control, and the simulation results are shown in Figs. 9 – 11.

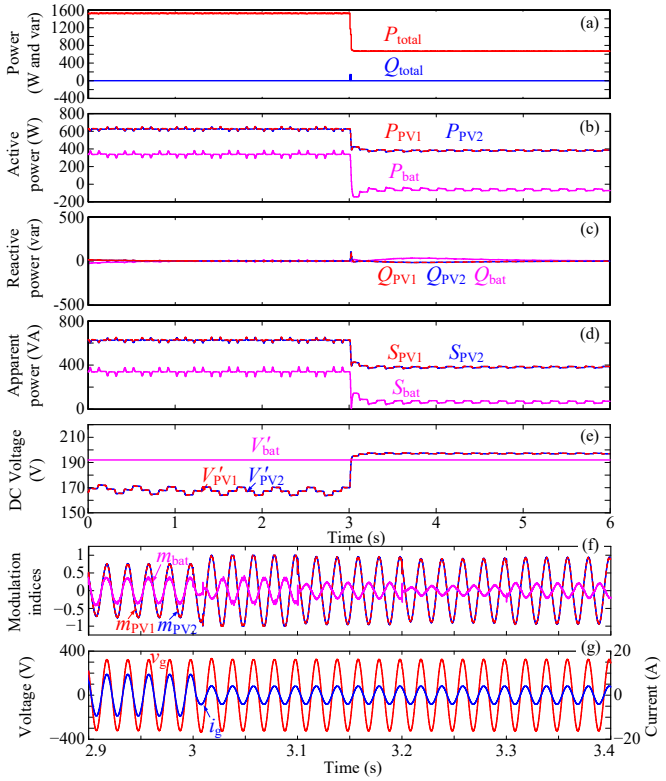

Fig. 9. Performance of the system during load active power step change, where $S_{PV,m}$ and $V'_{PV,m}$ denote the apparent power and the filtered DC voltage for the converter with PV#m, and S_{bat} and V'_{bat} denote the apparent power and filtered DC voltage for the battery converter: (a) total active and reactive power, (b) active power, (c) reactive power, (d) apparent power, (e) filter DC voltage, and (f) modulation indices for all converters, and (g) islanded grid voltage and load current.

Case 1: Firstly, the performance during the load active power step change is demonstrated in Fig. 9, where the active power jumps from 1520 W to 680 W at t = 3 s. As shown in Fig. 9, before t = 3 s, all PVs are operating in the MPPT mode, which can be confirmed by Fig. 9(e), where the PV voltage oscillate around 170 V. The remaining 350-W power is supplied by the battery. After t = 3 s, because of the reduction of the line current, over-modulation of PV converters appears, as shown in Fig. 9(f). Therefore, a part of PV power is discarded to avoid this, and the PV voltages deviate from their MPP and increase to 197 V, as shown in Fig. 9(e). In the steady state, the active power for each PV converter reduces to 375 W, and the 70-W surplus power is absorbed by the battery. The AC voltage at the PCC are kept sinusoidal with high power quality during the entire process.

Case 2: The performance during the load reactive power step change is shown in Fig. 10, where the load reactive power jumps from 0 to 1600 var at t = 7 s. As shown in Fig. 10, the PV power increases to 520 W for each PV converter, and the battery is charged at 360 W. Since the PV converters are contributing more active power than the battery converter, more reactive power is supported by the battery converter. In steady state, 410 var reactive power is provided by each PV converter, and 780 var from the battery converter. The apparent power for the battery converter is also larger than the PV converters.

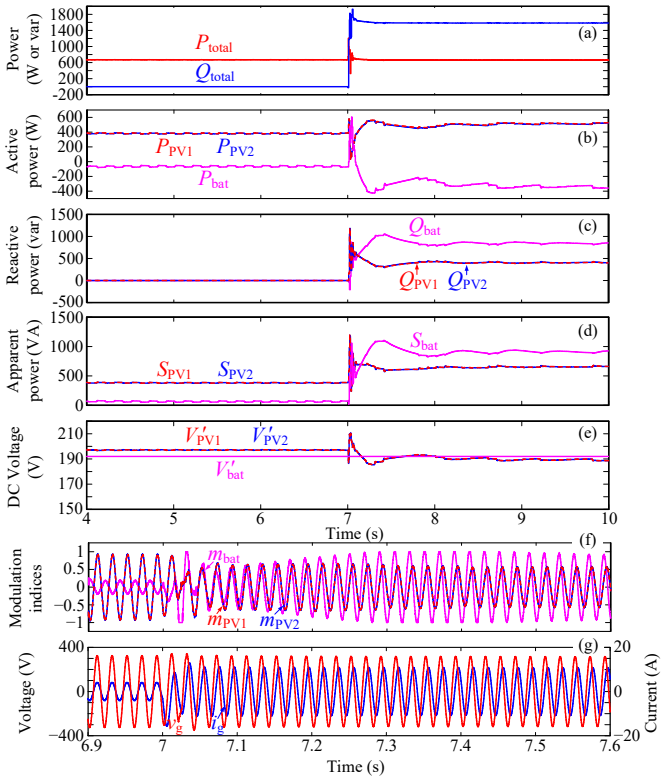

Fig. 10. Performance of the system during load reactive power step change: (a) total active and reactive power, (b) active power, (c) reactive power, (d) apparent power, (e) filter DC voltage, and (f) modulation indices for all converters, and (g) islanded grid voltage and load current.

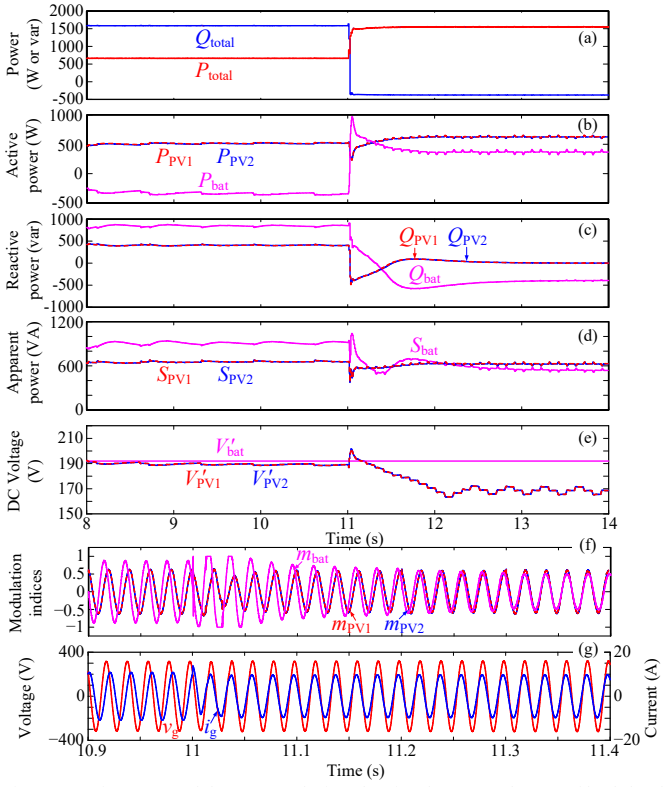

Fig. 11. Performance of the system during the simultaneous change of both load active and reactive power: (a) total active and reactive power, (b) active power, (c) reactive power, (d) apparent power, (e) filter DC voltage, and (f) modulation indices for all converters, and (g) islanded grid voltage and load current.

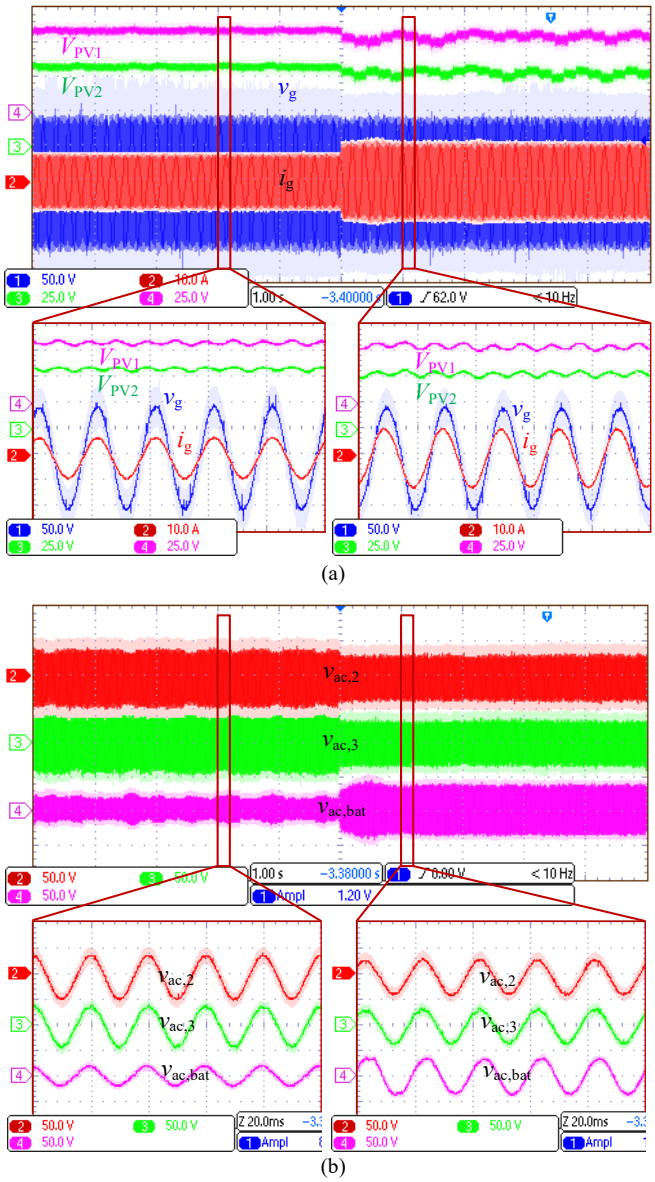

Fig. 12. Experimental results of an islanded series PVBH system shown in Fig. 1, where the AC load changes from 400 W to 600 W / 100 var (V_{PV1} and V_{PV2} [25 V/div]: DC voltages of PV #1 and #2; v_g [50 V/div]: grid voltage; i_g [10 A/div]: load current; $v_{ac,2}$, $v_{ac,3}$ and $v_{ac,bat}$ [50 V/div]: output voltages of the two PV converters and the battery converter).

Regardless of the over-modulation appeared on the first cycle after the load change, over-modulation re-appeared on the battery converter at t = 7.3 s because of the lower PF. Consequently, the PV voltages slightly increases afterwards, and the modulation index for the battery converter retreat back to the linear modulation region. The entire system is stable during the load change, except the two cycles after the load change, where v_g is slightly distorted, the islanded AC voltage is kept in high power quality.

Case 3: To demonstrate the control performance when both load active and reactive power change, simulation results are shown in Fig. 11, where the load active power changes from 680 W to 1650 W, and load reactive power changes from 1600 var to −380 var. In steady state, all PV converters operate

in the MPPT mode again, with the PV voltages oscillating around 170 V, and active power being around 625 W. The battery converter switches from the charging mode to discharging mode to provide the remaining 400-W power. Due to the unequal active power contribution, all reactive power is provided by the battery converter, and approximately equal apparent power sharing is realized in steady state. To overcome the over-modulation appeared after the load change, PV voltages are slightly increased during the transient, as shown in Fig. 11(e). The phase angle difference between the islanded AC voltage and the load current indicates that the system is operating from the quadrant I to quadrant IV. The AC voltage is kept in high quality in both transient and steady-state conditions.

B. Experimental results

To further validate the effectiveness of the proposed control, experiments have also been performed on a down-scaled 3-cell series PVBH system, which is assembled with three Infineon FS50R12KT4_B15 IGBT modules. One Keysight E4360A PV simulator was used to provide the power supply for two PV converters, and one Delta Elektronika SM330 DC power supply paralleling with a resistor bank is adopted to mimic the battery behavior. Three TMS320F28335 digital signal processors were employed as the individual controllers, which are interlinked with the RS-485 serial communications. The baud-rate is selected as 9600 bps. Most parameters same as the simulation, except that 1) the rated PV power for each converter cell is 275 W, 2) the nominal AC voltage is reduced to 70 V due to the limited output voltage of the PV simulator, 3) the battery nominal voltage is reduced to 48 V, and 4) the MPPT sampling-rate is reduced to 5 Hz.

Fig. 12 demonstrates the experimental results when the islanding AC load changes from 400 W to 600 W / −100 var. After the load step change, the two PVs operate at their maximum power points, as shown in Fig. 12(a), where the DC voltage of PV #1 and #2 oscillate around 55 V. The reactive power is redistributed among the three cells according to their active power contribution, and in steady state, the apparent power for all converters are roughly the same. This can be confirmed from Fig. 12(b), where the AC voltage amplitude for all three converters are similar. Since the same line current flows through all converters, the apparent power is approximately equally distributed among the three converters. During the entire process, the islanding AC voltage is stable and of high quality.

V. CONCLUSIONS

A novel decentralized control for the series PVBH system was proposed in this digest. Firstly, a PQ decoupling control method was introduced, which enables the individual PQ control of each converter with only local measurements. Then, a reactive power distribution scheme was proposed to balance the loading of all converters. To prevent the over-modulation, two AOM loops were developed. Compared with conventional communication-based methods, only several variables with slow dynamics should be transmitted by the LBC in the proposed approach, which greatly reduces the communication burden and increases the communication fault-tolerance of the series system. Simulation and experimental results have validated the effectiveness of the proposed method.

REFERENCES

[1] J. He, Y. Li, C. Wang, Y. Pan, C. Zhang, and X. Xing, "Hybrid microgrid with parallel- and series-connected microconverters," *IEEE Trans. Power Electron*., vol. 33, no. 6, pp. 4817-4831, June 2018.

[2] L. Liu, H. Li, Z. Wu, and Y. Zhou, "A cascaded photovoltaic system integrating segmented energy storages with self-regulating power allocation control and wide range reactive power compensation," *IEEE Trans. Power Electron*., vol. 26, no. 12, pp. 3545-3559, Dec. 2011.

[3] A. Marquez, J. I. Leon, S. Vazquez, L. G. Franquelo, and S. Kouro, "Operation of an hybrid PV-battery system with improved harmonic performance," in *Proc. 43rd Annu. Conf. IEEE Ind. Electron. Soc*., 2017, pp. 4272–4277.

[4] Y. Pan, A. Sangwongwanich, Y. Yang and F. Blaabjerg, "A phase-shifting MPPT to mitigate interharmonics from cascaded H-bridge PV inverters," IEEE Trans. Ind. Appl., DOI: 10.1109/TIA.2020.3000969.

[5] J. He, Y. Li, B. Liang, and C. Wang, "Inverse power factor droop control for decentralized power sharing in series-connected-microconverters-based islanding microgrids," *IEEE Trans. Ind. Electron*., vol. 64, no. 9, pp. 7444-7454, Sept. 2017.

[6] Y. Sun, G Shi, X Li, W Yuan, M Su, H Han, and X Hou, "An f-P/Q droop control in cascaded-type microgrid," *IEEE Trans. Power Syst*., vol. 33, no. 1, pp. 1136-1138, Jan. 2018.

[7] H. Jafarian, R. Cox, J. H. Enslin, S. Bhowmik, and B. Parkhideh, "Decentralized active and reactive power control for an AC-stacked PV inverter with single member phase compensation," *IEEE Trans. Ind. Appl*., vol. 54, no. 1, pp. 345-355, Jan.-Feb. 2018.

[8] P.-H. Wu, Y.-C. Su, J.-L. Shie and P.-T. Cheng, "A distributed control technique for the multilevel cascaded converter," *IEEE Trans. Ind. Appl*., vol. 55, no. 2, pp. 1649-1657, Mar.-Apr. 2019.

[9] Y. Pan, C. Zhang, S. Yuan, A. Chen, and J. He, "A decentralized control method for series connected PV battery hybrid microgrid," in *Proc. IEEE Transp. Electrific. Conf. Expo, Asia-Pacific (ITEC Asia-Pacific)*, Aug. 2017, pp. 1–6.

[10] Q. Zhang, and K. Sun, "A flexible power control for PV-battery hybrid system using cascaded H-bridge converters," *IEEE J. Emerg. Sel. Topics Power Electron*., vol. 7, no. 4, pp. 2184-2195, Dec. 2019.

[11] N. Kim and B. Parkhideh, "Control and operating range analysis of an AC-stacked PV inverter architecture integrated with a battery," *IEEE Trans. Power Electron*., vol. 33, no. 12, pp. 10032-10037, Dec. 2018.

[12] H. Liao, X. Zhang, and X. Hou, "A decentralized control of series-connected PV-ES inverters with MPPT and virtual inertia functionality," in *Proc. IEEE APEC Expo*., Mar. 2020, pp. 3221-3224.

[13] T. Zhao, X. Zhang, W. Mao, F. Wang, J. Xu, Y. Gu, and X. Wang, "An optimized third harmonic compensation strategy for single-phase cascaded H-bridge photovoltaic inverter," *IEEE Trans. Ind. Electron.*, vol. 65, no. 11, pp. 8635-8645, Nov. 2018.